Loss of ATF6α in a Human Carcinoma Cell Line Is Compensated not by Its Paralogue ATF6β but by Sustained Activation of the IRE1 and PERK Arms for Tumor Growth in Nude Mice

AUTHOR(S):

Jin, Shengyu; Jin, Byungseok; Ishikawa, Tokiro; Ninagawa, Satoshi; Okada, Tetsuya; Koyasu, Sho; Harada, Hiroshi; Mori, Kazutoshi

CITATION:

Jin, Shengyu ...[et al]. Loss of ATF6α in a Human Carcinoma Cell Line Is Compensated not by Its Paralogue ATF6β but by Sustained Activation of the IRE1 and PERK Arms for Tumor Growth in Nude Mice. Molecular Biology of the Cell 2023, 34(3): ar20.

ISSUE DATE:

2023-03

URL:

http://hdl.handle.net/2433/283997

MBoC | ARTICLE

Loss of ATF6α in a human carcinoma cell line is compensated not by its paralogue ATF6β but by sustained activation of the IRE1 and PERK arms for tumor growth in nude mice

Shengyu Jin[a], Byungseok Jin[a], Tokiro Ishikawa[a], Satoshi Ninagawa[a,†], Tetsuya Okada[a], Sho Koyasu[a,‡], Hiroshi Harada[b], and Kazutoshi Mori[a,*]

[a]Department of Biophysics, Graduate School of Science, Kyoto University, Kyoto 606-8502, Japan; [b]Laboratory of Cancer Cell Biology, Graduate School of Biostudies, Kyoto University, Kyoto 606-8501, Japan

ABSTRACT **To survive poor nutritional conditions, tumor cells activate the unfolded protein response, which is composed of the IRE1, PERK, and ATF6 arms, to maintain the homeostasis of the endoplasmic reticulum, where secretory and transmembrane proteins destined for the secretory pathway gain their correct three-dimensional structure. The requirement of the IRE1 and PERK arms for tumor growth in nude mice is established. Here we investigated the requirement for the ATF6 arm, which consists of ubiquitously expressed ATF6α and ATF6β, by constructing ATF6α-knockout (KO), ATF6β-KO, and ATF6α/β-double KO (DKO) in HCT116 cells derived from human colorectal carcinoma. Results showed that these KO cells grew similarly to wild-type (WT) cells in nude mice, contrary to expectations from our analysis of ATF6α-KO, ATF6β-KO, and ATF6α/β-DKO mice. We then found that the loss of ATF6α in HCT116 cells resulted in sustained activation of the IRE1 and PERK arms in marked contrast to mouse embryonic fibroblasts, in which the loss of ATF6α is compensated for by ATF6β. Although IRE1-KO in HCT116 cells unexpectedly did not affect tumor growth in nude mice, IRE1-KO HCT116 cells with ATF6α knockdown grew significantly more slowly than WT or IRE1-KO HCT116 cells. These results have unraveled the situation-dependent differential compensation strategies of ATF6α.**

Monitoring Editor
Anne Spang
University of Basel

Received: Jul 26, 2022
Revised: Jan 3, 2023
Accepted: Jan 19, 2023

INTRODUCTION

Soluble and transmembrane proteins destined for the secretory pathway are synthesized at ribosomes attached to the endoplasmic reticulum (ER). Usually these proteins are efficiently folded and matured with assistance from molecular chaperones and folding enzymes (collectively termed ER chaperones hereafter) abundantly expressed in the luminal side of the ER. However, proteins that remain unfolded or misfolded are recognized and dealt with by ER-associated degradation (ERAD), which culminates in ubiquitination-dependent degradation by the cytosolic proteasome (Bukau *et al.*, 2006). Under a variety of physiological and pathological conditions, however, this quality control system is compromised, resulting in ER stress characterized as the accumulation of unfolded or misfolded proteins in the ER. To cope with ER stress, a ubiquitous cellular mechanism, termed the unfolded protein response (UPR), is activated to maintain the homeostasis of the ER (Kaufman, 1999; Mori, 2000).

The UPR is triggered when three types of transmembrane proteins in the ER, namely, IRE1, PERK, and ATF6, sense ER stress and initiate their downstream transcriptional and translational programs (Mori, 2009; Walter and Ron, 2011). Translation is generally regulated at the level of initiation. Thus phosphorylation of the α subunit of

This article was published online ahead of print in MBoC in Press (http://www.molbiolcell.org/cgi/doi/10.1091/mbc.E22-07-0292) on January 25, 2023.

Present address: †Biosignal Research Center, Kobe University, 1-1, Rokkodai-cho, Nada-ku, Kobe 657-8501, Japan; ‡Current address: Department of Diagnostic Imaging and Nuclear Medicine, Graduate School of Medicine, Kyoto University, Kyoto 606-8501, Japan.

*Address correspondence to: Kazutoshi Mori (mori@upr.biophys.kyoto-u.ac.jp).

Abbreviations used: CRT, calreticulin; eIF2, eukaryotic initiation factor 2; DKO, double knockout; ER, endoplasmic reticulum; ERAD, ER-associated degradation; ERSE, ER stress response element; KD, knockdown; KO, knockout; MEFs, mouse embryonic fibroblasts; PBS, phosphate-buffered saline; TALEN, transcription activatorlike effector nuclease; UPR, unfolded protein response; UPRE, UPR element; WT, wild type.

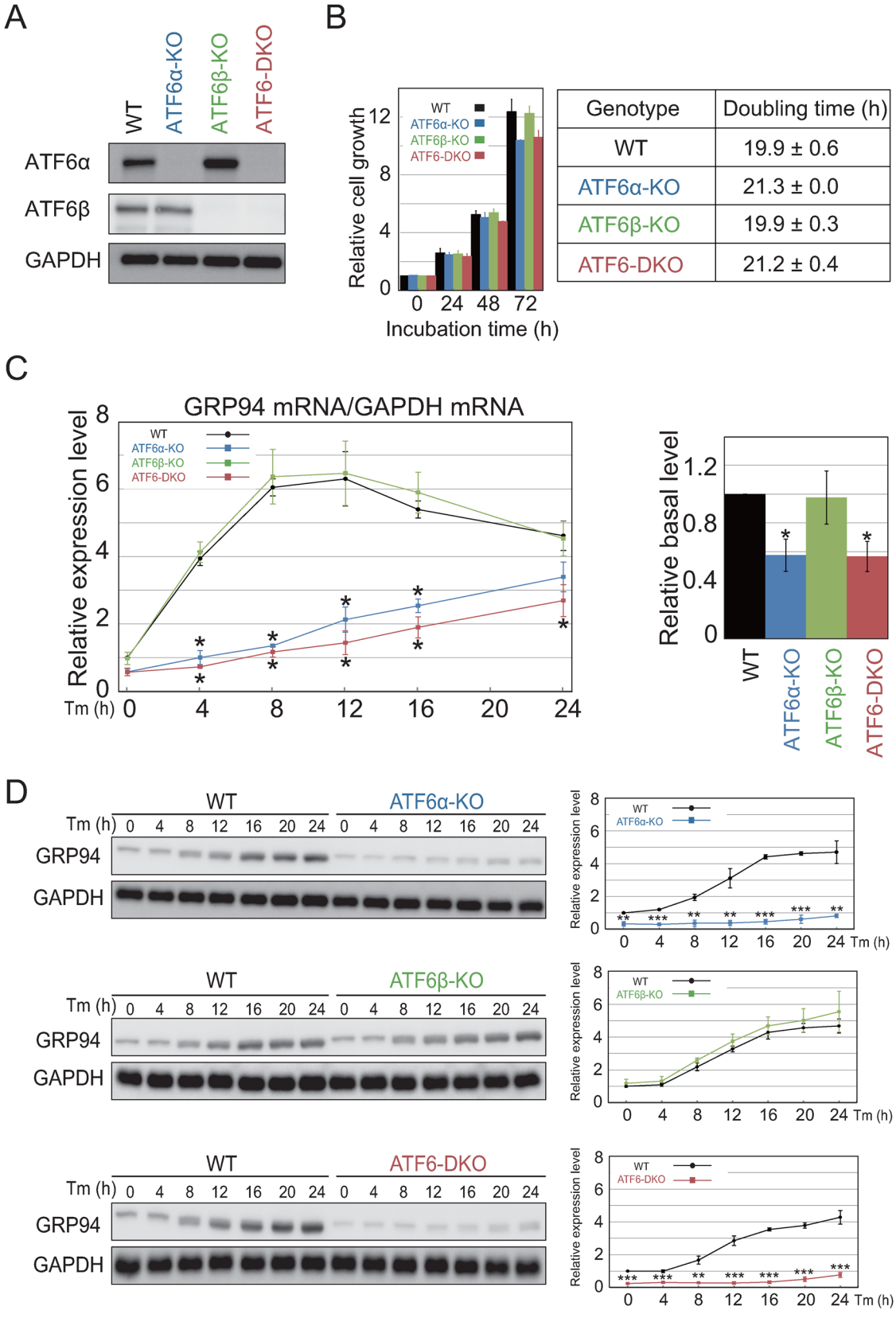

Genotype	Doubling time (h)
WT	19.9 ± 0.6
ATF6α-KO	21.3 ± 0.0
ATF6β-KO	19.9 ± 0.3
ATF6-DKO	21.2 ± 0.4

FIGURE 1: Effect of ATF6α/β deletion on induction of GRP94. (A) Cell lysates were prepared from HCT116 cells of the indicated genotypes and analyzed by immunoblotting using anti-ATF6α, anti-ATF6β, and anti-GAPDH antibodies. (B) Growth of HCT116 cells of the indicated genotypes was determined by counting cell number every 24 h, and their doubling times were determined ($n = 3$). (C) HCT116 cells of the indicated genotypes were treated with tunicamycin (Tm, 2 μg/ml) for the indicated time, and then total RNA was isolated and subjected to quantitative RT-PCR to determine the level of GRP94 mRNA relative to that of GAPDH mRNA ($n = 3$). The levels of GRP94 mRNA at time 0 in

eukaryotic initiation factor 2 (eIF2α) leads to transient and global attenuation of translation (Harding *et al.*, 2002). The major transcriptional targets for maintenance of the homeostasis of the ER are ER chaperones and ERAD components. Two types of ER stress-responsive *cis*-acting elements have been identified: the ER stress response element (ERSE), composed of CCAAT-N9-CCACG, is responsible for transcriptional induction of ER chaperones (Yoshida *et al.*, 1998), whereas the UPR element (UPRE), composed of TGACGTGG/A, is involved in the transcriptional induction of ERAD components (Yoshida *et al.*, 2001a).

IRE1, consisting of ubiquitous IRE1α (Tirasophon *et al.*, 1998) and gut-specific IRE1β (Wang *et al.*, 1998) in mammals, is a type I transmembrane protein possessing protein kinase and endoribonuclease domains in its cytosolic side. It is the most evolutionarily conserved UPR sensor/transducer from yeast to humans (Cox *et al.*, 1993; Mori *et al.*, 1993). Its downstream transcription factor is encoded by XBP1 mRNA in metazoans. Upon activation in response to ER stress via oligomerization and autophosphorylation, IRE1 initiates unconventional (frame switch-type) splicing of XBP1 mRNA to produce a highly active transcription factor XBP1(S) which stands for spliced form (Yoshida *et al.*, 2001a; Calfon *et al.*, 2002), whereas constitutively expressed unspliced XBP1 mRNA is translated to produce XBP1(U) (U stands for unspliced form), which can function as a negative regulator of XBP1(S) (Yoshida *et al.*, 2006). XBP1(S) binds to both ERSE and UPRE (Yoshida *et al.*, 2001a).

PERK is a ubiquitously expressed type I transmembrane protein possessing a protein kinase domain in its cytosolic side, which is conserved in metazoans. Upon activation in response to ER stress via oligomerization and autophosphorylation, PERK phosphorylates eIF2α to decrease the burden on the ER by attenuating translation (Harding *et al.*, 1999). Interestingly and paradoxically, attenuated translation leads to translational induction of certain mRNAs, including ATF4 mRNA encoding the transcription factor ATF4. Targets of ATF4 contain the proapoptotic transcription factor CHOP (Harding *et al.*, 2000).

ATF6, consisting of both ubiquitous ATF6α and ATF6β, is a type II transmembrane protein which has gained functionality as a transcription factor in vertebrates (Haze *et al.*, 1999, 2001; Ishikawa *et al.*, 2013). Constitutively synthesized ATF6α(P) and ATF6β(P) (P stands for precursor form) relocate from the ER to the Golgi apparatus in response to ER stress via COPII vesicles and are then sequentially cleaved by two proteases, Site-1 and Site-2 proteases (Ye *et al.*, 2000; Nadanaka *et al.*, 2004). ATF6α(N) and ATF6β(N) (N stands for nuclear form) liberated from the Golgi membrane contain DNA-binding and transcriptional activation domains and activate transcription via binding to ERSE (Yoshida *et al.*, 2000, 2001b). ATF6α(N) is more active than ATF6β(N) as a transcription factor (Haze *et al.*, 2001). In addition, ATF6α(N)-XBP1(S) heterodimer binds to UPRE with higher affinity than XBP1(S) homodimer (Yamamoto *et al.*, 2007).

Mouse embryonic fibroblasts (MEFs) deficient in ATF6α, ATF6β, IRE1α, or XBP1 were obtained and extensively characterized. BiP/GRP78 and GRP94 are two major ER chaperones of the Hsp70 and Hsp90 family, respectively, and react with anti-KDEL antibody. Northern blotting or quantitative RT-PCR showed that induction of BiP mRNA in response to ER stress was greatly attenuated in ATF6α-knockout (KO) MEFs (Wu *et al.*, 2007; Yamamoto *et al.*, 2007) but was not affected in ATF6β-KO MEFs (Yamamoto *et al.*, 2007), IRE1α-KO MEFs (Yoshida *et al.*, 2003; Wu *et al.*, 2007), or XBP1-KO MEFs (Lee *et al.*, 2003). Microarray analysis showed that the targets of ATF6α include various molecular chaperones (BiP, GRP94, ORP150/GRP170, and calreticulin [CRT]), the co-chaperone ERdj3, and various oxidoreductases (ERp72, P5, GRP58, and ERO1β) (Adachi *et al.*, 2008). Immunoblotting confirmed that induction of BiP, GRP94, ERp72, and P5 was lost in ATF6α-KO MEFs (Wu *et al.*, 2007; Yamamoto *et al.*, 2007). Northern blotting confirmed that induction of ERdj3 mRNA was greatly attenuated in ATF6α-KO MEFs (Adachi *et al.*, 2008). Interestingly, Northern blotting showed that the co-chaperone ERdj4 mRNA was induced in response to ER stress similarly in both wild-type (WT) and ATF6α-KO MEFs (Adachi *et al.*, 2008), and that induction of ERdj4 mRNA was lost in XBP1-KO MEFs (Lee *et al.*, 2003). These results indicate that a majority of ER chaperones are targets of ATF6α, whereas the co-chaperones ERdj3 and ERdj4 are targets of the ATF6 and IRE1 arms, respectively (Yamamoto *et al.*, 2007; Adachi *et al.*, 2008).

Microarray analysis also showed that ERAD components (HRD1, SEL1L, Herp1, Derlin3, and EDEM1) are targets of ATF6α (Adachi *et al.*, 2008). Northern blotting or quantitative RT-PCR showed that induction of mRNA encoding HRD1, Herp1, and EDEM1 was greatly attenuated not only in ATF6α-KO MEFs but also in IRE1α-KO MEFs and XBP1-KO MEFs (Wu *et al.*, 2007; Yamamoto *et al.*, 2008). Based on these findings, we postulated that a majority of ERAD components are induced by ATF6α-XBP1 heterodimer (Yamamoto *et al.*, 2007, 2008).

Tumor cells must cope with conditions of hypoxia and poor nutrition until the completion of angiogenesis. To do so, they activate the hypoxia response and UPR to survive (Akman *et al.*, 2021; Satija *et al.*, 2021). Accordingly, virally transformed XBP1-KO MEFs and PERK-KO MEFs, in which activation of the IRE1 and PERK arms, respectively, in response to ER stress was completely prevented, were shown to grow very poorly in nude mice (Romero-Ramirez *et al.*, 2004; Bi *et al.*, 2005). In contrast, nothing is known regarding the ATF6 arm, because ATF6α and ATF6β function redundantly in the ATF6 arm and their double KO (DKO) MEFs are not available due to embryonic lethality in ATF6α/ATF6β-DKO mice at a very early stage (Yamamoto *et al.*, 2007).

Here we examined the effect of deletion of the ATF6 arm on tumor growth in nude mice following the advent of innovative genome editing technologies which allowed us to construct ATF6α/ATF6β-DKO in a human carcinoma cell line.

RESULTS

Deletion of ATF6α but not ATF6β results in sustained activation of the IRE1 and PERK arms

We previously constructed ATF6α- and ATF6β-DKO (ATF6-DKO) cells using HCT116 diploid cells derived from human colorectal carcinoma (Koba *et al.*, 2020) via the construction of ATF6α- and ATF6β-KO cells (Supplemental Figure S1, A and 1B). Data for genomic PCR confirming homologous recombination induced by the transcription activator-like effector nuclease (TALEN) method in ATF6α-KO and ATF6β-KO cells are shown in Supplemental Figure S1, C and D, respectively. The absence of ATF6α in ATF6α-KO and ATF6-DKO cells and that of ATF6β in ATF6β-KO and ATF6-DKO cells were confirmed by immunoblotting (Figure 1A). WT and these

various KO cells relative to that in WT cells are shown on the right. (D) HCT116 cells of the indicated genotypes were treated with tunicamycin (Tm, 2 μg/ml) for the indicated time, and then cell lysates were prepared and analyzed by immunoblotting using anti-KDEL antibody to determine the level of GRP94 relative to that of GAPDH ($n = 3$). Quantified data are shown on the right.

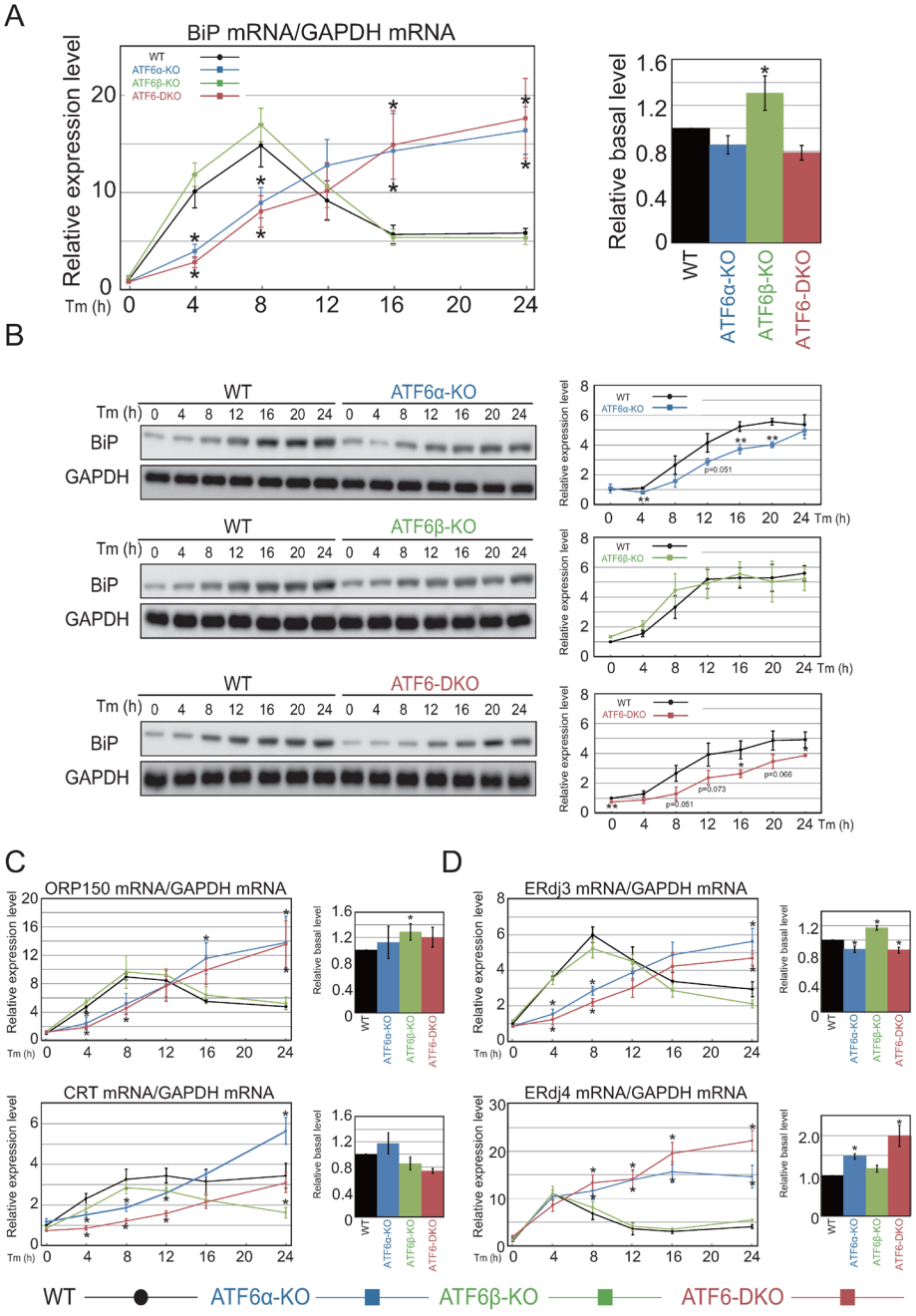

FIGURE 2: Effect of ATF6α/β deletion on induction of ER chaperones and co-chaperones. (A) Quantitative RT-PCR was conducted to determine the level of BiP mRNA relative to that of GAPDH mRNA ($n = 3$), as in Figure 1C. (B) Immunoblotting using anti-KDEL antibody was conducted to determine the level of BiP relative to that of GAPDH ($n = 3$), as in Figure 1D. (C) Quantitative RT-PCR was conducted to determine the levels of ORP150 mRNA and CRT mRNA relative to that of GAPDH mRNA ($n = 3$), as in Figure 1C. (D) Quantitative RT-PCR was conducted to determine the levels of ERdj3 mRNA and ERdj4 mRNA relative to that of GAPDH mRNA ($n = 3$), as in Figure 1C.

three types of KO cells grew in a comparable manner in cell culture (Figure 1B).

Quantitative RT-PCR (Figure 1C) and immunoblotting (Figure 1D) revealed that induction of GRP94 in response to treatment with tunicamycin, which induces ER stress by inhibiting protein *N*-glycosylation (Kaufman, 1999), observed in WT cells was greatly attenuated in ATF6α-KO and ATF6-DKO cells but not in ATF6β-KO cells at the levels of mRNA and protein, respectively, similarly to the case of MEFs deficient in ATF6α or ATF6β (Yamamoto *et al.*, 2007). In contrast, quantitative RT-PCR revealed that although induction of BiP mRNA observed in WT cells was significantly decreased in ATF6α-KO and ATF6-DKO cells but not in ATF6β-KO cells until 8 h, it rather increased significantly from 16 h in ATF6α-KO and ATF6-DKO cells (Figure 2A). Accordingly, induction of BiP protein observed in WT cells was only slightly decreased in ATF6α-KO and ATF6-DKO cells, whereas it was unaffected in ATF6β-KO cells (Figure 2B). Induction of ORP150 mRNA and CRT mRNA showed a pattern similar to that of BiP mRNA, except for reproducibly lower induction of CRT mRNA in ATF6-DKO cells compared with ATF6α-KO cells at all time points as well as a higher level of CRT mRNA in WT cells compared with ATF6β-KO cells after 12 h for an unknown reason (Figure 2C).

Induction of ERdj3 mRNA, a target of the ATF6 arm, in response to tunicamycin treatment in WT, ATF6α-KO, ATF6β-KO, and ATF6-DKO cells showed a pattern similar to that of BiP mRNA (Figure 2D). In contrast, induction of ERdj4 mRNA, a target of the IRE1 arm, observed in WT cells in response to tunicamycin treatment was not decreased in ATF6α-KO, ATF6β-KO, or ATF6-DKO cells until 4 h but then increased rather significantly from 8 h in ATF6α-KO and ATF6-DKO cells but not in ATF6β-KO cells (Figure 2D). These results suggested the possibility that the IRE1 arm is activated in ATF6α-KO and ATF6-DKO cells.

We therefore checked the activation status of IRE1α by immunoblotting using standard and phos-tag gels and found that activation of IRE1α via autophosphorylation (thus with slower migration during SDS–PAGE) peaked at 4 h in WT and ATF6β-KO cells, whereas the activation status of IRE1α was markedly sustained in ATF6α-KO and ATF6-DKO cells (Figure 3A). Accordingly, transient induction of the active (spliced) form of XBP1, designated XBP1(S), after tunicamycin treatment in WT and ATF6β-KO cells was markedly sustained in ATF6α-KO and ATF6-DKO cells (Figure 3B). Of note, the extent of cleavage of Caspase3, an apoptosis marker, was increased in tunicamycin-treated ATF6α-KO and ATF6-DKO cells compared with that in tunicamycin-treated WT and ATF6β-KO cells (Figure 3C), suggesting that sustained induction of XBP1(S) appeared not to be protective for ATF6α-KO and ATF6-DKO cells.

We also found that the activation of PERK via autophosphorylation (thus with slower migration during SDS–PAGE) peaked at 4 h in WT and ATF6β-KO cells, whereas the activation status of PERK was

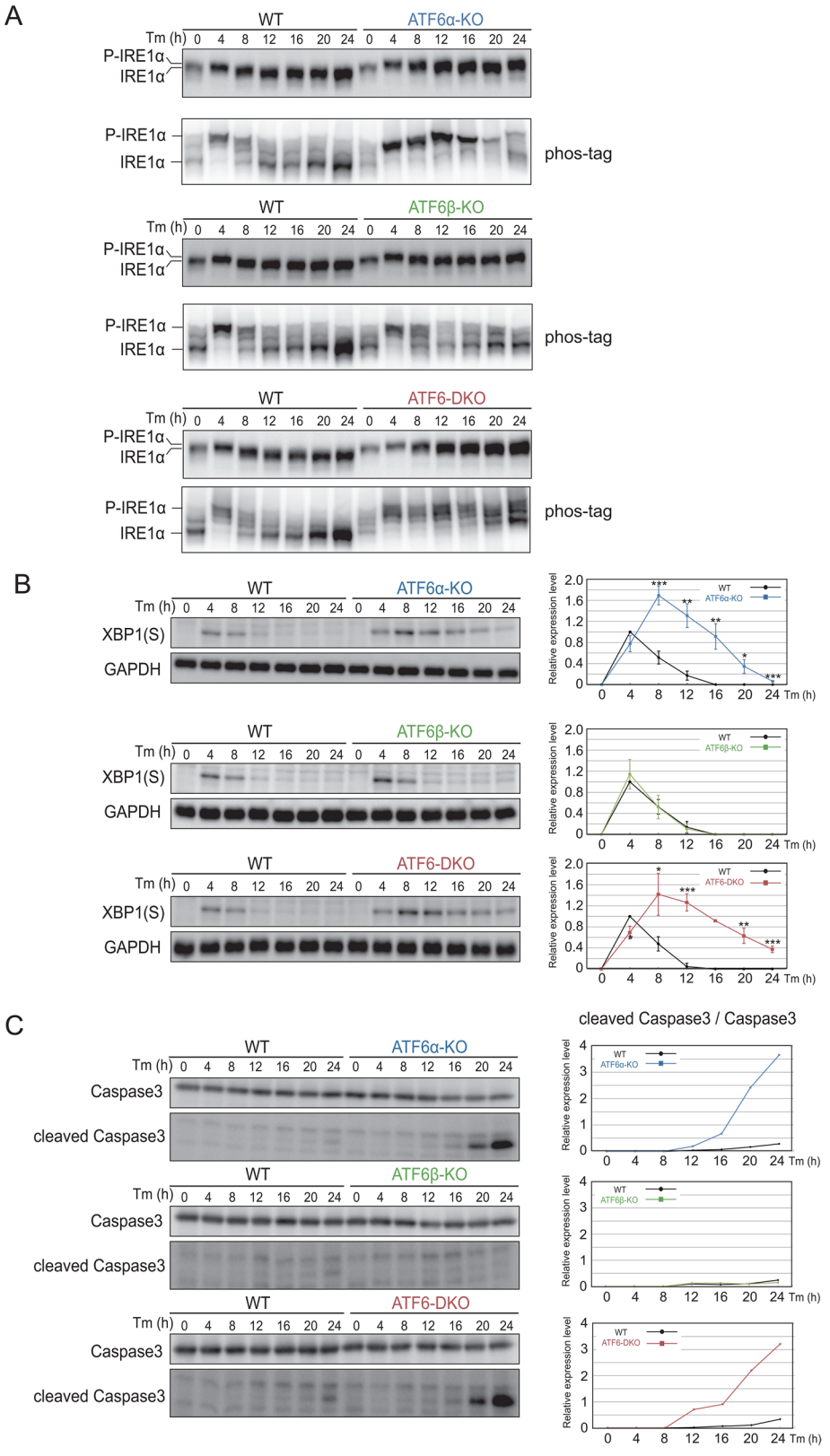

FIGURE 3: Effect of ATF6α/β deletion on activation status of IRE1α, induction of XBP1(S), and cleavage of Caspase3. (A) Immunoblotting of cell lysates run in standard and phos-tag gels was conducted using anti-IRE1α antibody to determine the activation status of IRE1α, as in Figure 1D. (B) Immunoblotting using anti-XBP1 antibody was conducted to determine the level of XBP1(S) relative to that of GAPDH ($n = 3$), as in Figure 1D. (C) Immunoblotting using anti-caspase3 and anti-cleaved caspae3 antibodies was conducted to determine the cleavage of caspase3, as in Figure 1D.

sustained in ATF6α-KO and ATF6-DKO cells (Figure 4A). Accordingly, transient induction of ATF4 and CHOP after tunicamycin treatment in WT and ATF6β-KO cells was markedly sustained in ATF6α-KO and ATF6-DKO cells (Figure 4, B and C)

We injected WT, ATF6α-KO, ATF6β-KO, and ATF6-DKO cells into nude mice and found that the absence of ATF6α and ATF6β did not affect the growth of HCT116 cells in these mice (Figure 5).

Simultaneous IRE1α-KO and ATF6α-knockdown (KD) inhibits tumor growth in nude mice

To determine the significance of sustained activation of IRE1α in the absence of ATF6α on tumor growth, we intended to knock out both IRE1α and ATF6α in HCT116 cells. We constructed IRE1α-KO cells using the TALEN method (Supplemental Figure S2, A and B). After removing the puromycin-resistant gene from IRE1α-KO cells using Cre-LoxP recombination to obtain IRE1α-KO* cells, the introduction of targeting and TALEN vectors for ATF6α into IRE1α-KO* cells produced two independent (#26 and #41) colonies (Supplemental Figure S2, C and D). As immunoblotting showed that the level of ATF6α in #26 and #41 was approximately one-fourth and one-tenth, respectively, of that in WT cells (Supplemental Figure S2E), we used #41 as IRE1α-KO*/ATF6α-KD cells hereafter. The absence of IRE1α in IRE1α-KO* and IRE1α-KO*/ATF6α-KD cells was confirmed by immunoblotting (Figure 6A). IRE1α-KO* and IRE1α-KO*/ATF6α-KD cells grew significantly more slowly in cell culture compared with HCT116 cells with other genotypes (Figure 6B), Detailed characterization of IRE1α-KO cells, IRE1α-KO* cells, and IRE1α-KO*/ATF6α-KD cells (Supplemental Figures S2, F and G, and S3, A, B, and C) is described in *Materials and Methods*.

XBP1(S) was not induced at all in response to tunicamycin treatment in IRE1α-KO* and IRE1α-KO*/ATF6α-KD cells, as expected (Figure 6C), whereas sustained induction of ATF4 and CHOP was maintained in tunicamycin-treated IRE1α-KO* and IRE1α-KO*/ATF6α-KD cells (Figure 6, D and E). It should be noted that because transcription of CHOP was regulated by both the PERK and the ATF6 arms (Yoshida *et al.*, 2000; Ma *et al.*, 2002), the extent of induction of CHOP mRNA in response to tunicamycin treatment was significantly lower in IRE1α-KO*/ATF6α-KD cells than in IRE1α-KO* cells (Figure 6E). More extensive cleavage of Caspase3 was observed in tunicamycin-treated IRE1α-KO*/ATF6α-KD

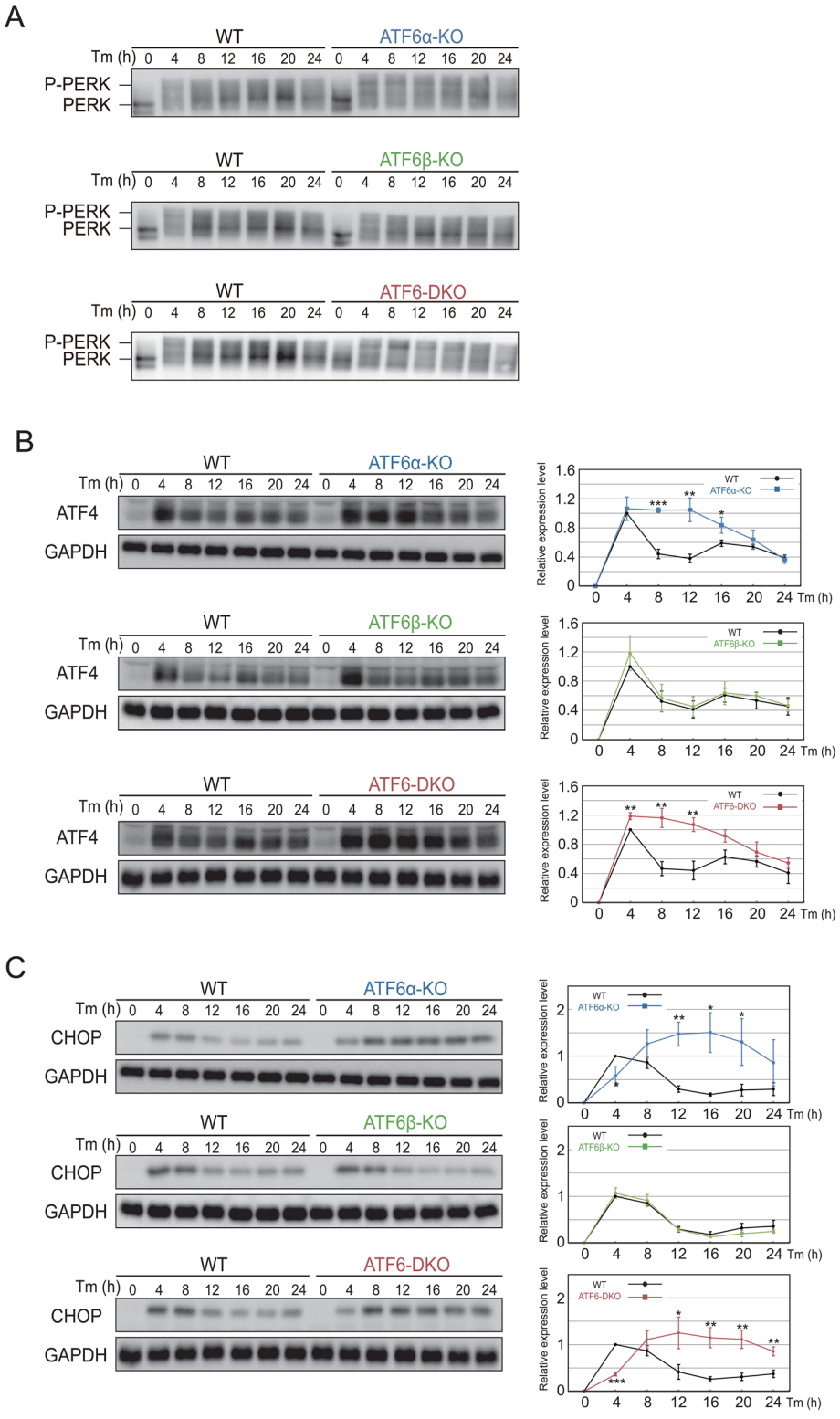

FIGURE 4: Effect of ATF6α/β deletion on activation status of PERK, induction of ATF4, and induction of CHOP. (A) Immunoblotting using anti-PERK antibody was conducted to determine the activation status of PERK, as in Figure 1D. (B) Immunoblotting using anti-ATF4 antibody was conducted to determine the level of ATF4 relative to that of GAPDH ($n = 3$), as in Figure 1D. (C) Immunoblotting using anti-CHOP antibody was conducted to determine the level of CHOP relative to that of GAPDH ($n = 3$), as in Figure 1D.

cells compared with tunicamycin-treated IRE1α-KO* cells (Supplemental Figure S3D), suggesting the protective role of ATF6α.

Quantitative RT-PCR revealed that induction of mRNA coding for ER chaperones BiP, ORP150 and CRT as well as ER co-chaperone ERdj3—all of which are targets of the ATF6 arm—in response to tunicamycin treatment was slightly decreased in IRE1α-KO* cells, whereas induction of ERdj4 mRNA, a target of the IRE1 arm, in response to tunicamycin treatment was lost almost completely in IRE1α-KO* and IRE1α-KO*/ATF6α-KD cells, as expected (Figure 7A, purple lines). Importantly, sustained induction of mRNA coding for BiP, ORP150, CRT and ERdj3 observed in ATF6α-KO cells (Figure 7A, blue lines) was canceled in IRE1α-KO*/ATF6α-KD cells (Figure 7A, pink lines). Accordingly, induction of BiP protein was decreased more evidently in IRE1α-KO*/ATF6α-KD cells (Figure 7B) compared with ATF6α-KO and ATF6-DKO cells (Figure 2B). Although induction of GRP94 mRNA and GRP94 protein was not decreased in IRE1α-KO* cells, it was lost in IRE1α-KO*/ATF6α-KD cells (Figure 7, A and C), similarly to the case of ATF6α-KO and ATF6-DKO cells (Figure 1, C and D).

Injection experiments revealed that IRE1α-KO* cells grew in nude mice similarly to WT and ATF6α-KO cells (Figure 8), although IRE1α-KO* cells grew significantly more slowly in cell culture than WT and ATF6α-KO cells (Figure 6B). Critically, IRE1α-KO*/ATF6α-KD cells grew significantly more slowly in nude mice than IRE1α-KO* cells (Figure 8), although they grew similarly in cell culture (Figure 6B).

DISCUSSION

The requirement of ubiquitously expressed IRE1α and PERK for tumor growth in nude mice was reported within 6 years after the discovery of these molecules (Romero-Ramirez *et al.*, 2004; Bi *et al.*, 2005). In contrast, the role of the ATF6 arm in tumor growth in nude mice has not been determined for more than 20 years since its discovery, except for one report showing reduced tumor growth in nude mice by KD of ATF6α in D-HEp3 cells, which had been reprogrammed into a reversible dormant phenotype during passage in culture for more than 40 generations from the highly tumorigenic and metastatic human squamous carcinoma cell line T-Hep3 (Schewe and Aguirre-Ghiso, 2008). This is because the ATF6 arm consists of both ubiquitously expressed

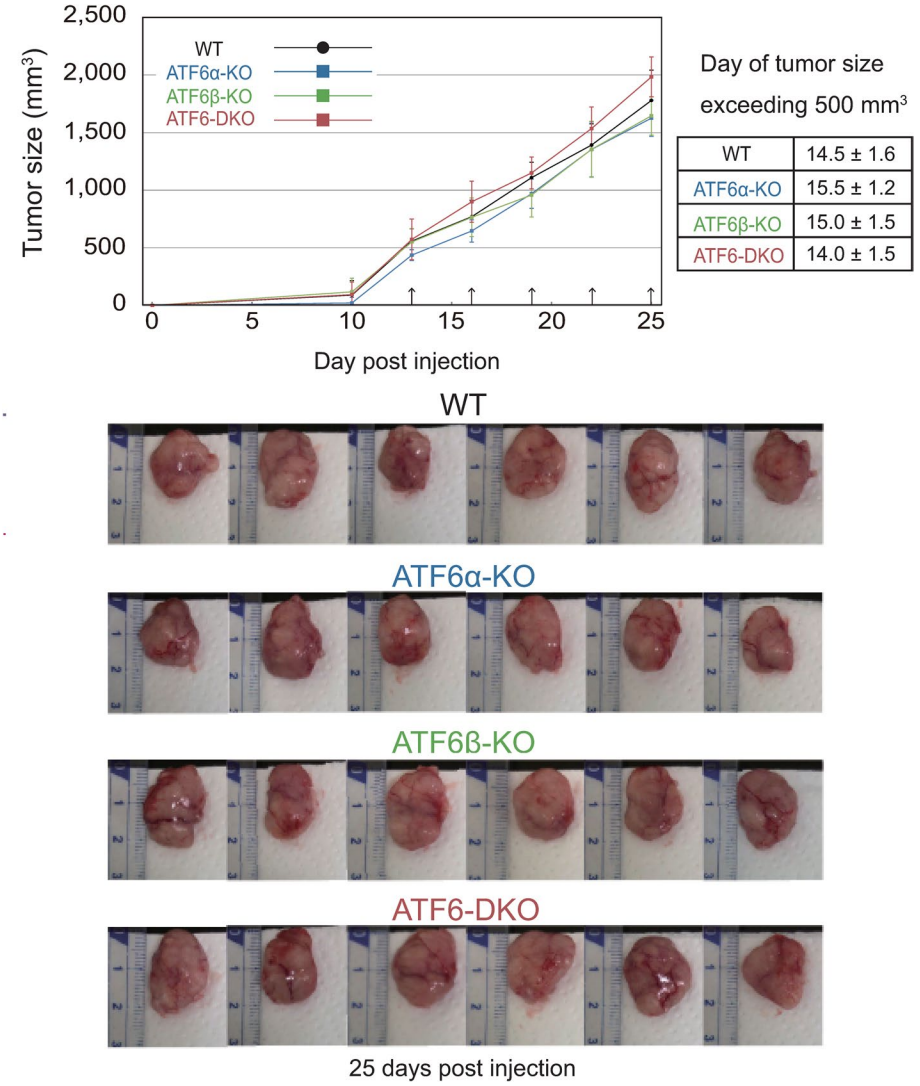

FIGURE 5: Effect of ATF6α/β deletion on tumor growth in nude mice. Tumor sizes were measured on the days indicated by arrows after injection of HCT116 cells of the indicated genotypes into nude mice. The day on which tumor size exceeded 500 mm^3 was determined and is shown in Table (n = 6). Tumors formed 25 d postinjection were photographed.

ATF6α and ATF6β. ATF6α- or ATF6β-single KO mice or medaka fish showed no obvious phenotype, whereas ATF6α- and ATF6β-DKO mice or medaka fish exhibited embryonic lethality at very early stages (Yamamoto *et al.*, 2007; Ishikawa *et al.*, 2013). This hampered production of ATF6α- and ATF6β-DKO MEFs for viral transformation. We further showed that both ATF6α and ATF6β responded to physiological ER stress, which occurred during embryonic development of medaka fish by activating the major ER chaperone BiP promoter (Ishikawa *et al.*, 2013). Based on these findings, it has been considered that construction of ATF6α- and ATF6β-DKO cancer cells is essential to examine the requirement of the ATF6 arm for tumor growth in nude mice.

Here we constructed ATF6α-KO, ATF6β-KO, and ATF6α/ATF6β-DKO in tumorigenic HCT116 cells. Results showed that ATF6α-KO cells and ATF6α/ATF6β-DKO cells responded to tunicamycin treatment quite similarly in the induction of various ER chaperones (Figures 1 and 2). In other words, ATF6β played no role in the response to tunicamycin treatment in HCT116 cells, just like ATF6β-KO MEFs and ATF6β-KO medaka fish responded to tunicamycin treatment similarly to WT MEFs and WT fish, respectively (Yamamoto *et al.*, 2007; Ishikawa *et al.*, 2013). In contrast to our expectation, ATF6α/ATF6β-DKO HCT116 cells grew normally in nude mice (Figure 5). This was due to sustained activation of IRE1α and PERK in the absence of ATF6α (Figure 3 and 4). Indeed, when ATF6α was knocked down in IRE1α-KO HCT116 cells, these cells grew significantly more slowly than ATF6α-KO or IRE1α-KO HCT116 cells in nude mice (Figure 8). KO or KD of PERK in IRE1α-KO/ATF6α-KD cells is expected to further slow their growth in nude mice.

We were surprised to find that the loss of IRE1α in HCT116 cells did not affect tumor growth in nude mice (Figure 8), because we previously showed that virally transformed MEFs deficient in XBP1, a transcription factor downstream of IRE1α, did not grow at all in nude mice (Romero-Ramirez *et al.*, 2004). A literature search revealed that IRE1α KO in human triple negative breast cancer cell lines, such as MDA-MB-231 and HCC1806 cells (Harnoss *et al.*, 2020), or in the human multiple myeloma cell line KMS-11 (Harnoss *et al.*, 2019), reduced tumor growth in nude mice. Treatment of the human multiple myeloma cell line RPMI8226 with the IRE1α inhibitor MKC-3946 (Mimura *et al.*, 2012) or STF083010 (Papandreou *et al.*, 2011) reduced tumor growth in nude mice, whereas treatment of MDA-MB-231 cells with the IRE1α inhibitor MKC8866 did not do so (Logue *et al.*, 2018). IRE1α KD in the human prostate cancer cell line LNCaP and treatment of human prostate cancer cell lines such as LNCaP, VCap, 22Rv1, and C4-2B with the IRE1α inhibitor MKC8866 (Sheng *et al.*, 2019) reduced tumor growth in nude mice (Sheng *et al.*, 2015). Therefore, the case of HCT116 cells appears to be exceptional. We will examine the effect of XBP1 KO in HCT116 cells on tumor growth in nude mice, and if XBP1-KO HCT116 cells do not grow well in nude mice, we will then examine which of XBP1(S) or XBP1(U) helps the growth of IRE1α-KO HCT116 cells in these mice.

Current and previous analyses of cells deficient in ATF6α have revealed a marked difference in the response to tunicamycin treatment between HCT116 cells and MEFs (Yamamoto *et al.*, 2007), namely, that sustained activation of IRE1α and PERK occurs only in HCT116 cells. Our preliminary experiments suggest that this might be due to a difference in the level of protein synthesis between colorectal carcinoma-derived cells and primary embryonic fibroblasts. The effect of ATF6α KD on the IRE1 and PERK arms was previously examined using human neuroblastoma-derived SH-SY5Y cells (Walter *et al.*, 2018). Since measurement of fluorescent protein expression from reporter genes in ER-stressed cells showed up-regulation of the IRE1 arm but no effect on the PERK arm in ATF6α-KD SH-SY5Y cells, the authors focused only on the IRE1 arm and determined the underlying mechanism at the mRNA and protein levels, resulting in the proposal that IRE1

Reagent type or resources	Designation	Source or reference	Identifier	Additional information
Cell line (*Homo Sapiens*)	colorectal carcinoma	ATCC	HCT116	The cell lines have been authenticated and tested negative for mycoplasma.
Antibody	anti-KDEL (Mouse monoclonal)	MBL	Cat#: M181-3	WB (1:5000)
Antibody	anti-GAPDH (Rabbit polyclonal)	Trevigen	Cat#:2275-PC-100	WB (1:1000)
Antibody	anti-IRE1α (Rabbit monoclonal)	Cell Signaling Technology	Cat#: 3294	WB (1:1000)
Antibody	anti-XBP1 (Rabbit polyclonal)	Santa Cruz Biotechnology	Cat#: sc-7160	WB (1:1000)
Antibody	Anti-PERK	Cell Signaling Technology	Cat#: 3192	WB (1:1000)
Antibody	anti-ATF4 (Rabbit polyclonal)	Santa Cruz Biotechnology	Cat#: sc-200	WB (1:1000)
Antibody	anti-CHOP (Rabbit polyclonal)	Santa Cruz Biotechnology	Cat#: sc-793	WB (1:1000)
Antibody	anti-Caspase-3 (Rabbit polyclonal)	Cell Signaling Technology	Cat#: 9662	WB (1:1000)
Antibody	anti-Cleaved Caspase-3 (Rabbit polyclonal)	Cell Signaling Technology	Cat#:9661	WB (1:1000)

TABLE 1: Key resources.

signaling during ER stress has an ATF6α-dependent "off-switch." However, our analysis at the protein level clearly showed sustained activation of both the IRE1 and PERK arms in ATF6α-KO HCT116 cells (Figures 3 and 4). We speculate that the level of protein synthesis in SH-SY5Y cells may be in between that in HCT116 cells and MEFs.

Here is our scenario for the differential compensation strategies of ATF6α. Transcriptional induction of ER chaperones is the most effective and productive way to cope with ER stress as it leads to the refolding of unfolded or misfolded proteins accumulated in the ER. This induction is mediated by the IRE1 arm in yeast and nonvertebrates, but the mediator is switched to the ATF6 arm in vertebrates (Mori, 2009). KO of the ATF6 arm produces the most detrimental effect on the development of both medaka fish and mice compared with KO of the IRE1 or PERK arm (Mori, 2009; Ishikawa *et al.*, 2013; Ishikawa *et al.*, 2017). We thus envision that switching to the ATF6 arm simultaneously requires a compensation strategy for its absence to maintain the viability of embryos of medaka fish and mice. We consider that this strategy is found in the duplication of the ATF6 gene to the ATF6α and ATF6β genes. Certain types of proteins synthesized in large amounts during embryonic development of medaka fish and mice, such as extracellular matrix proteins, perhaps cause physiological ER stress, which could be handled by various ER chaperones induced by ATF6α and ATF6β in a redundant manner (Ishikawa *et al.*, 2013).

In contrast, the level of protein synthesis is expected to be elevated in tumor cells compared with MEFs. Accordingly, perhaps a variety of proteins become unfolded or misfolded during tumor growth in nude mice, just as in cells treated with tunicamycin. In this case, the loss of ATF6α cannot be compensated for by its paralogue ATF6β but is compensated for by sustained activation of the IRE1α and PERK arms, which trigger their own signaling cascades to cope with "heavy" ER stress. Namely, the living organism must adopt situation-dependent differential compensation for the loss of ATF6α as a survival strategy under various stressful conditions.

MATERIALS AND METHODS

Request a protocol through *Bio-protocol*.

Statistics

Statistical analysis was conducted using Student's *t* test for the immunoblotting data, with probability expressed as $*p < 0.05$, $**p < 0.01$, and $***p < 0.001$, and using Dunnett test for the quantitative RT-PCR and tumor growth data in nude mice, with probability expressed as $*p < 0.05$.

Construction of plasmids

Recombinant DNA techniques were performed according to standard procedures (Sambrook *et al.*, 1989). The integrity of all constructed plasmids was confirmed by extensive sequencing analyses.

Cell culture and transfection

HCT116 cells (CCL-247; ATCC, Table 1) were cultured in DMEM (4.5 g/l glucose) supplemented with 10% fetal bovine serum, 2 mM glutamine, and antibiotics (100 U/ml penicillin and 100 μg/ml streptomycin) at 37°C in a humidified 5% CO_2/95% air atmosphere. Cells were transfected with plasmid DNA using polyethylenimine MAX (Polysciences) unless indicated and then incubated at 37°C for an appropriate time to express the transfected gene.

Construction of IRE1α targeting vector

The 1.5-kb fragment of the IRE1α gene used for the 3′-arm was amplified by PCR from HCT116 cell genomic DNA using the primers 5′-AGCGTCAGCAGCAGCAGCAG-3′ and 5′-ATTCGCCCTATAGTGAGTCG-3′ and then inserted between the NotI and the HindIII sites of the DT-A-pA/loxP/PGK-Puro-pA/loxP vector (Ninagawa *et al.*, 2014) to create the DT-A-pA/loxP/PGK-Puro-pA/loxP-3′-arm (IRE1α). The 1.5-kb fragment of the IRE1α gene used for the 5′-arm was similarly amplified using the primers 5′-CGCGCCTTAAGTCGACAAGC-3′ and 5′-CTGTCCTCCACCCCACGCTC-3′ and then inserted between the XbaI and the XhoI sites of DT-A-pA/loxP/PGK-Puro-pA/loxP-3′-arm (IRE1α) to create pKO-IRE1α-puromycin.

Construction of IRE1α-KO* and IRE1α-KO*/ATF6α-KD cells

pKO-IRE1α-puromycin as well as TALEN 5′ and 3′ target vectors for IRE1α (Supplemental Figure S2A) were transfected into HCT116 WT

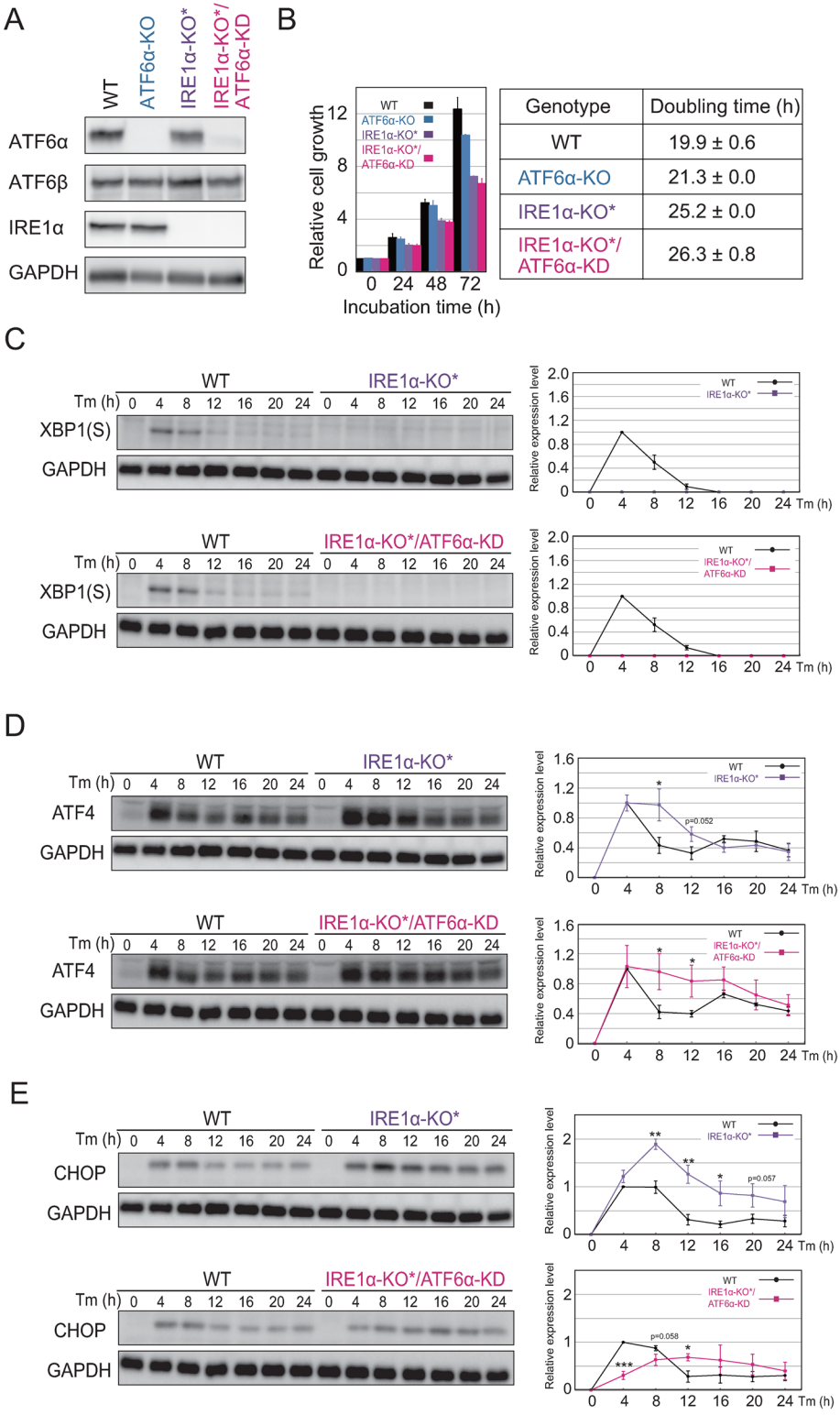

Genotype	Doubling time (h)
WT	19.9 ± 0.6
ATF6α-KO	21.3 ± 0.0
IRE1α-KO*	25.2 ± 0.0
IRE1α-KO*/ ATF6α-KD	26.3 ± 0.8

FIGURE 6: Effect of KD of ATF6α with simultaneous deletion of IRE1α on induction of XBP1(S), ATF4, and CHOP. (A) Cell lysates were prepared from HCT116 cells of the indicated genotypes and analyzed by immunoblotting using anti-ATF6α, anti-ATF6β, anti-IRE1α, and anti-GAPDH antibodies. The puromycin-resistant gene was removed from IRE1α-KO cells to produce IRE1α-KO* cells. (B) Growth of HCT116 cells of the indicated genotypes was determined by counting cell number every 24 h, and their doubling times were determined ($n = 3$). (C) Immunoblotting using anti-XBP1 antibody was conducted to determine the level of XBP1(S) relative to that of GAPDH ($n = 3$), as in Figure 1D. (D) Immunoblotting using anti-ATF4 antibody was conducted to determine the level of ATF4 relative to that of GAPDH ($n = 3$), as in Figure 1D. (E) Immunoblotting using anti-CHOP antibody was conducted to determine the level of CHOP relative to that of GAPDH ($n = 3$), as in Figure 1D.

cells using Lipofectamine LTX (Invitrogen). Transfected cells were selected in DMEM containing puromycin (0.5 μg/ml). Puromycin-resistant colonies were isolated and the IRE1α-KO cell line was identified by immunoblotting and genomic PCR (Supplemental Figure S2B).

Because a puromycin-resistant gene was used to select IRE1α-KO and ATF6α-KO cells (Supplemental Figures S1A and 2A), the puromycin-resistant gene was removed from the IRE1α-KO cell line by transfection of pANMerCreMer-hyg (Kikuchi *et al.*, 2013) using Lipofectamine LTX, followed by treatment with 200 μM tamoxifen (Merck) to create the IRE1α-KO* cell line; the removal of this puromycin-resistant gene in IRE1α-KO* cells was confirmed by genomic PCR (Supplemental Figure S2D).

Subsequently, pKO-ATF6α-puromycin as well as TALEN 5′ and 3′ target vectors for ATF6α were transfected into IRE1α-KO* cells using Lipofectamine LTX. Transfected cells were selected in DMEM containing puromycin (0.5 μg/ml). Puromycin-resistant colonies were isolated and the IRE1α-KO*/ATF6α-KD cell lines (#26 and #41) were identified by immunoblotting and genomic PCR (Supplemental Figure S2, E and F). Genomic PCR produced the two bands designated [Puro-] and [deletion] from the ATF6α locus in IRE1α-KO*/ATF6α-KD cells (Supplemental Figure S2F). Sequencing revealed that the band [Puro-] in IRE1α-KO*/ATF6α-KD cells lacked two nucleotides downstream of the initiation codon, resulting in the production of no functional protein, whereas the band [deletion] in IRE1α-KO*/ATF6α-KD cells lacked 1039 nucleotides, including the entire exon 1, resulting in the production of ATF6α of 620 aa (Supplemental Figure S3A) because of translation starting from the ATG codon present in exon 3 (Supplemental Figure S3, A and B). The shorter ATF6α (aa51-670) was *N*-glycosylated because it produced after tunicamycin treatment migrated faster during SDS–PAGE [Supplemental Figure S3, Ca] and because it was sensitive to digestion with endoglycosidase H (Endo H) [Supplemental Figure S3, Cb], demonstrating that the shorter ATF6α is present in the ER with correct orientation. Shorter ATF6α(N) produced from shorter ATF6α(P) after

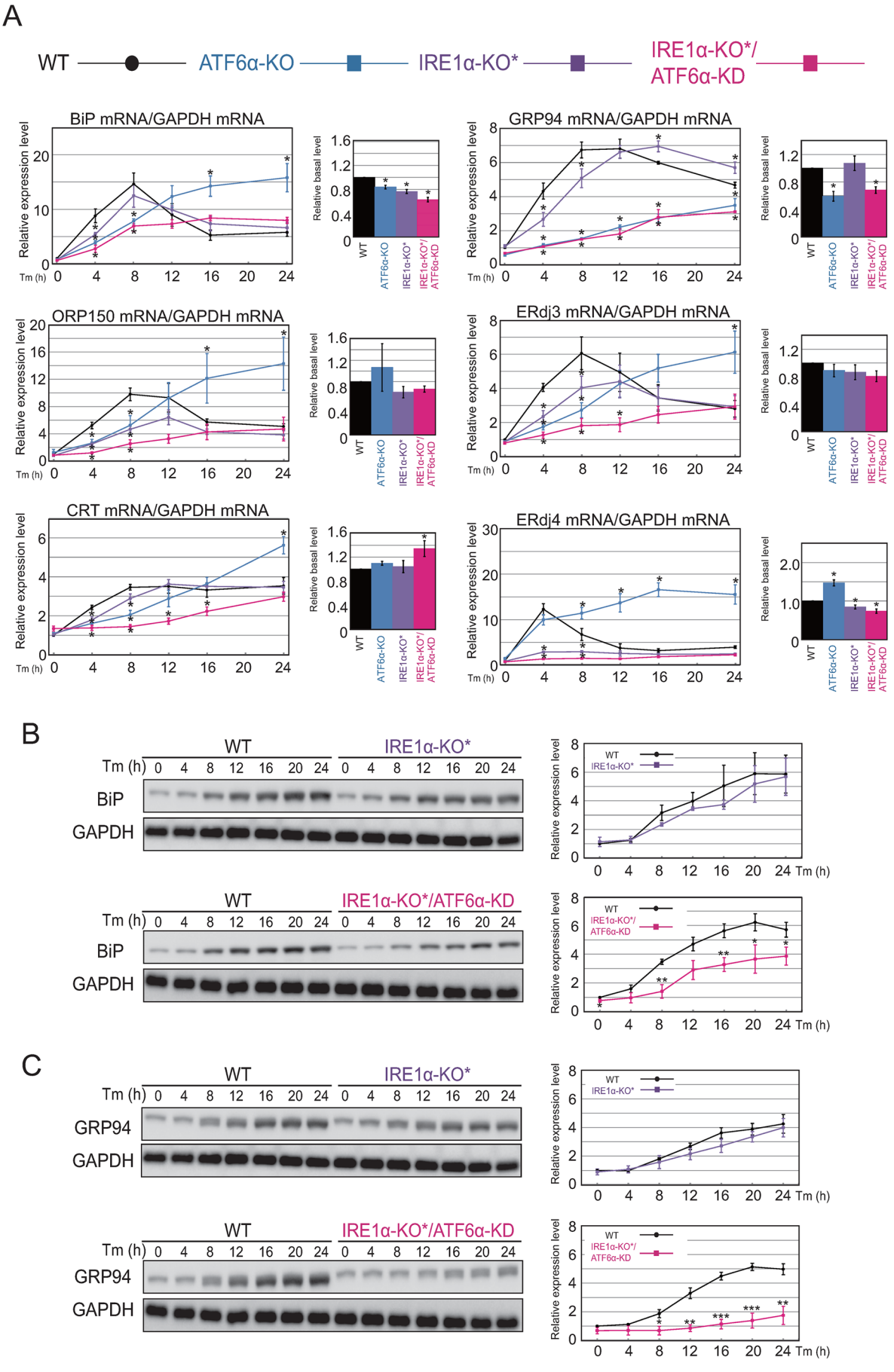

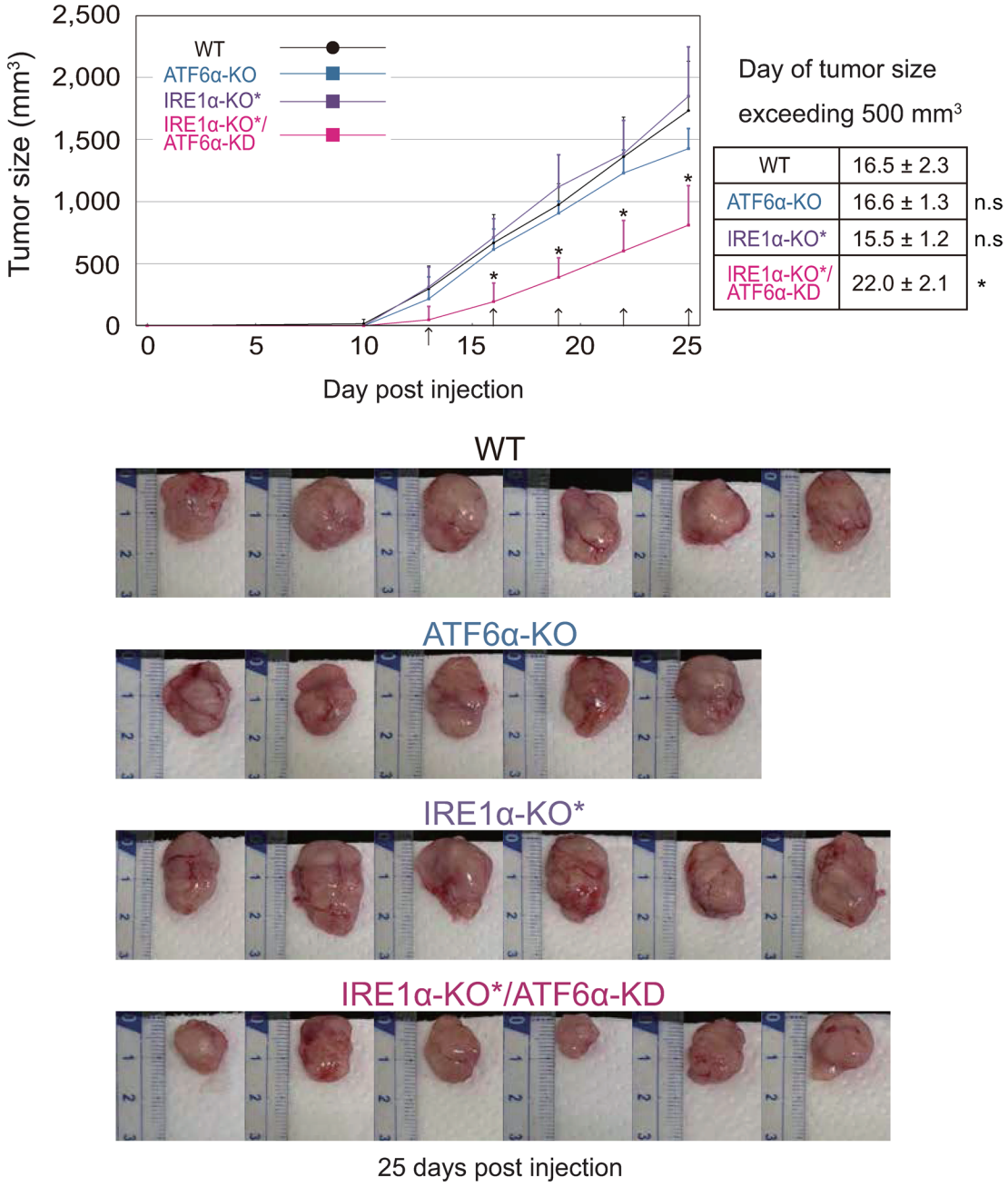

FIGURE 8: Effect of KD of ATF6α with simultaneous deletion of IRE1α on tumor growth in nude mice. Tumor sizes were measured on the days indicated by arrows after injection of HCT116 cells of the indicated genotypes into nude mice. The day on which tumor size exceeded 500 mm^3 was determined and is shown in Table ($n = 6$, except $n = 5$ for ATF6α-KO). Tumors formed 25 d postinjection were photographed.

tunicamycin treatment of IRE1α-KO*/ATF6α-KD cells was below the level of detection by immunoblotting [Supplemental Figure S3Ca].

Immunoblotting

HCT116 cells were washed with ice-cold phosphate-buffered saline (PBS) and lysed in 300 µl of 1% NP-40 buffer (50 mM Tris/HCl,

FIGURE 7: Effect of KD of ATF6α with simultaneous deletion of IRE1α on induction of ER chaperones and co-chaperones. (A) Quantitative RT-PCR was conducted to determine the levels of BiP mRNA, GRP94 mRNA, ORP150 mRNA, CRT mRNA, ERdj3 mRNA, and ERdj4 mRNA relative to that of GAPDH mRNA ($n = 3$), as in Figure 1C. (B) Immunoblotting using anti-KDEL antibody was conducted to determine the level of BiP relative to that of GAPDH ($n = 3$), as in Figure 1D. (C) Immunoblotting using anti-KDEL antibody was conducted to determine the level of GRP94 relative to that of GAPDH ($n = 3$), as in Figure 1D.

pH 7.5, containing 1% NP-40, 150 mM NaCl, protease inhibitor cocktail [Nacalai Tesque], 10 μM MG132 and 10 mM N-ethylmaleimide). Lysates were clarified by centrifugation at 14,000 rpm for 10 min at 4°C. Cleared lysates were mixed with 2× Laemmli's SDS sample buffer with 200 mM dithiothreitol and boiled for 5 ~ 10 min. Prepared cell lysates were subjected to SDS–PAGE followed by immunoblotting, which was carried out according to the standard procedure (Sambrook *et al.*, 1989) using Western Blotting Luminol Reagent (Santa Cruz Biotechnology) and antibodies described in Table 1. Chemiluminescence was detected using an LAS-3000mini LuminoImage analyzer (Fujifilm). ATF6α and ATF6β were detected with rabbit anti-ATF6α (Haze *et al.*, 1999) and anti-ATF6β (Haze *et al.*, 2001) polyclonal antibodies, respectively. Phos-tag gels were obtained from Fujifilm (#199-17391), and samples were run in running buffer (Tris base 0.5 M, MOPS 0.5 M, 0.5% SDS, $NaHSO_3$ 0.5 M, pH 7.8) at 30 mA for 180 min at 4°C.

Genomic PCR

HCT116 cells were washed with ice-cold PBS, suspended in alkaline lysis reagent A (25 mM NaOH and 0.2 mM EDTA), boiled for 10 min, and then mixed with an equivalent volume of alkaline lysis regent B (40 mM Tris/HCl, pH 8.0). Homologous recombination in HCT116 cells was confirmed by genomic PCR using a pair of primers described in Supplemental File S1.

Quantitative RT-PCR

Total RNA prepared from cultured cells (~5×10^6 cells) by the acid guanidinium/phenol/chloroform method using ISOGEN (Nippon Gene) was converted to cDNA using Moloney murine leukemia virus reverse transcription (Invitrogen) and random primers and then subjected to quantitative RT-PCR analysis using the SYBR Green method (Applied Biosystems) and a pair of primers described in Supplemental File S1.

Transplantation into nude mice

HCT116 cells of various genotypes (5×10^6 cells in 50 μl PBS) were subcutaneously transplanted into the right hind legs of athymic nude mice (BALB/c nu/nu; Japan SLC. Inc., Hamamatsu, Japan). The length (R) and breadth (r) of tumor were measured using an electronic caliper (AS ONE, 4-484-01), and the volume (V) of tumor was calculated as V = R x r x r/2. The animal experiments were approved by the Animal Research Committee of Kyoto University and performed according to guidelines governing animal care in Japan.

ACKNOWLEDGMENTS

The authors declare no competing financial interests. We thank Kaoru Miyagawa for her technical and secretarial assistance. This work was financially supported in part by grants from MEXT, Japan (18K06216 to S.N., 19K06658 to T.I., and 17H06419 to K.M.) and AMED-CREST, Japan (20gm1410005 to K.M.). A part of this study was conducted through the Joint Usage/Research Center Program of the Radiation Biology Center, Kyoto University, and the Core-to-Core Program from JSPS (JPJSCCA20200009).

REFERENCES

Adachi Y, Yamamoto K, Okada T, Yoshida H, Harada A, Mori K (2008). ATF6 is a transcription factor specializing in the regulation of quality control proteins in the endoplasmic reticulum. Cell Struct Funct 33, 75–89.

Akman M, Belisario DC, Salaroglio IC, Kopecka J, Donadelli M, De Smaele E, Riganti C (2021). Hypoxia, endoplasmic reticulum stress and chemoresistance: dangerous liaisons. J Exp Clin Cancer Res 40, 28.

Bi M, Naczki C, Koritzinsky M, Fels D, Blais J, Hu N, Harding H, Novoa I, Varia M, Raleigh J, *et al.* (2005). ER stress-regulated translation increases tolerance to extreme hypoxia and promotes tumor growth. EMBO J 24, 3470–3481.

Bukau B, Weissman J, Horwich A (2006). Molecular chaperones and protein quality control. Cell 125, 443–451.

Calfon M, Zeng H, Urano F, Till JH, Hubbard SR, Harding HP, Clark SG, Ron D (2002). IRE1 couples endoplasmic reticulum load to secretory capacity by processing the *XBP-1* mRNA. Nature 415, 92–96.

Cox JS, Shamu CE, Walter P (1993). Transcriptional induction of genes encoding endoplasmic reticulum resident proteins requires a transmembrane protein kinase. Cell 73, 1197–1206.

Harding HP, Calfon M, Urano F, Novoa I, Ron D (2002). Transcriptional and translational control in the mammalian unfolded protein response. Annu Rev Cell Dev Biol 18, 575–599.

Harding HP, Novoa II, Zhang Y, Zeng H, Wek R, Schapira M, Ron D (2000). Regulated translation initiation controls stress-induced gene expression in mammalian cells. Mol Cell 6, 1099–1108.

Harding HP, Zhang Y, Ron D (1999). Protein translation and folding are coupled by an endoplasmic-reticulum-resident kinase. Nature 397, 271–274.

Harnoss JM, Thomas AL, Reichelt M, Guttman O, Wu TD, Marsters SA, Shemorry A, Lawrence DA, Kan D, Segal E, *et al.* (2020). IRE1α Disruption in triple-negative breast cancer cooperates with antiangiogenic therapy by reversing ER stress adaptation and remodeling the tumor microenvironment. Cancer Res 80, 2368–2379.

Harnoss JM, Le Thomas A, Shemorry A, Marsters SA, Lawrence DA, Lu M, Chen YA, Qing J, Totpal K, Kan D, *et al.* (2019). Disruption of IRE1α through its kinase domain attenuates multiple myeloma. Proc Natl Acad Sci USA 116, 16420–16429.

Haze K, Okada T, Yoshida H, Yanagi H, Yura T, Negishi M, Mori K (2001). Identification of the G13 (cAMP-response-element-binding protein-related protein) gene product related to activating transcription factor 6 as a transcriptional activator of the mammalian unfolded protein response. Biochem J 355, 19–28.

Haze K, Yoshida H, Yanagi H, Yura T, Mori K (1999). Mammalian transcription factor ATF6 is synthesized as a transmembrane protein and activated by proteolysis in response to endoplasmic reticulum stress. Mol Biol Cell 10, 3787–3799.

Ishikawa T, Kashima M, Nagano AJ, Ishikawa-Fujiwara T, Kamei Y, Todo T, Mori K (2017). Unfolded protein response transducer IRE1-mediated signaling independent of XBP1 mRNA splicing is not required for growth and development of medaka fish. eLife 6, e26845.

Ishikawa T, Okada T, Ishikawa-Fujiwara T, Todo T, Kamei Y, Shigenobu S, Tanaka M, Saito TL, Yoshimura J, Morishita S, *et al.* (2013). ATF6alpha/beta-mediated adjustment of ER chaperone levels is essential for development of the notochord in medaka fish. Mol Biol Cell 24, 1387–1395.

Kaufman RJ (1999). Stress signaling from the lumen of the endoplasmic reticulum: coordination of gene transcriptional and translational controls. Genes Dev 13, 1211–1233.

Kikuchi K, Narita T, Pham VT, Iijima J, Hirota K, Keka IS, Mohiuddin KO, Hori T, Fukagawa T, Essers J, *et al.* (2013). Structure-specific endonucleases xpf and mus81 play overlapping but essential roles in DNA repair by homologous recombination. Cancer Res 73, 4362–4371.

Koba H, Jin S, Imada N, Ishikawa T, Ninagawa S, Okada T, Sakuma T, Yamamoto T, Mori K (2020). Reinvestigation of disulfide-bonded oligomeric forms of the unfolded protein response transducer ATF6. Cell Struct Funct 45, 9–21.

Lee AH, Iwakoshi NN, Glimcher LH (2003). XBP-1 regulates a subset of endoplasmic reticulum resident chaperone genes in the unfolded protein response. Mol Cell Biol 23, 7448–7459.

Logue SE, McGrath EP, Cleary P, Greene S, Mnich K, Almanza A, Chevet E, Dwyer RM, Oommen A, Legembre P, *et al.* (2018). Inhibition of IRE1 RNase activity modulates the tumor cell secretome and enhances response to chemotherapy. Nat Commun 9, 3267.

Ma Y, Brewer JW, Diehl JA, Hendershot LM (2002). Two distinct stress signaling pathways converge upon the CHOP promoter during the mammalian unfolded protein response. J Mol Biol 318, 1351–1365.

Mimura N, Fulciniti M, Gorgun G, Tai YT, Cirstea D, Santo L, Hu Y, Fabre C, Minami J, Ohguchi H, *et al.* (2012). Blockade of XBP1 splicing by inhibition of IRE1α is a promising therapeutic option in multiple myeloma. Blood 119, 5772–5781.

Mori K (2000). Tripartite management of unfolded proteins in the endoplasmic reticulum. Cell 101, 451–454.

Mori K (2009). Signalling pathways in the unfolded protein response: development from yeast to mammals. J Biochem 146, 743–750.

Mori K, Ma W, Gething MJ, Sambrook J (1993). A transmembrane protein with a cdc2+/CDC28-related kinase activity is required for signaling from the ER to the nucleus. Cell 74, 743–756.

Nadanaka S, Yoshida H, Kano F, Murata M, Mori K (2004). Activation of mammalian unfolded protein response is compatible with the quality control system operating in the endoplasmic reticulum. Mol Biol Cell 15, 2537–2548.

Ninagawa S, Okada T, Sumitomo Y, Kamiya Y, Kato K, Horimoto S, Ishikawa T, Takeda S, Sakuma T, Yamamoto T, Mori K (2014). EDEM2 initiates mammalian glycoprotein ERAD by catalyzing the first mannose trimming step. J Cell Biol 206, 347–356.

Papandreou I, Denko NC, Olson M, Van Melckebeke H, Lust S, Tam A, Solow-Cordero DE, Bouley DM, Offner F, Niwa M, Koong AC (2011). Identification of an Ire1alpha endonuclease specific inhibitor with cytotoxic activity against human multiple myeloma. Blood 117, 1311–1314.

Romero-Ramirez L, Cao H, Nelson D, Hammond E, Lee AH, Yoshida H, Mori K, Glimcher LH, Denko NC, Giaccia AJ, *et al*. (2004). XBP1 is essential for survival under hypoxic conditions and is required for tumor growth. Cancer Res 64, 5943–5947.

Sambrook J, Fritsch EF, Maniatis T (1989). Molecular Cloning: A Laboratory Manual. Cold Spring Harbor, NY: Cold Spring Harbor Laboratory Press.

Satija S, Kaur H, Tambuwala MM, Sharma P, Vyas M, Khurana N, Sharma N, Bakshi HA, Charbe NB, Zacconi FC, *et al*. (2021). Hypoxia-inducible factor (HIF): fuel for cancer progression. Curr Mol Pharmacol

Schewe DM, Aguirre-Ghiso JA (2008). ATF6alpha-Rheb-mTOR signaling promotes survival of dormant tumor cells in vivo. Proc Natl Acad Sci USA 105, 10519–10524.

Sheng X, Arnoldussen YJ, Storm M, Tesikova M, Nenseth HZ, Zhao S, Fazli L, Rennie P, Risberg B, Wæhre H, *et al*. (2015). Divergent androgen regulation of unfolded protein response pathways drives prostate cancer. EMBO Mol Med 7, 788–801.

Sheng X, Nenseth HZ, Qu S, Kuzu OF, Frahnow T, Simon L, Greene S, Zeng Q, Fazli L, Rennie PS, *et al*. (2019). IRE1α-XBP1s pathway promotes prostate cancer by activating c-MYC signaling. Nat Commun 10, 323.

Tirasophon W, Welihinda AA, Kaufman RJ (1998). A stress response pathway from the endoplasmic reticulum to the nucleus requires a novel bifunctional protein kinase/endoribonuclease (Ire1p) in mammalian cells. Genes Dev 12, 1812–1824.

Walter F, O'Brien A, Concannon CG, Düssmann H, Prehn JHM (2018). ER stress signaling has an activating transcription factor 6α (ATF6)-dependent "off-switch." J Biol Chem 293, 18270–18284.

Walter P, Ron D (2011). The unfolded protein response: from stress pathway to homeostatic regulation. Science 334, 1081–1086.

Wang XZ, Harding HP, Zhang Y, Jolicoeur EM, Kuroda M, Ron D (1998). Cloning of mammalian Ire1 reveals diversity in the ER stress responses. EMBO J 17, 5708–5717.

Wu J, Rutkowski DT, Dubois M, Swathirajan J, Saunders T, Wang J, Song B, Yau GD, Kaufman RJ (2007). ATF6alpha optimizes long-term endoplasmic reticulum function to protect cells from chronic stress. Dev Cell 13, 351–364.

Yamamoto K, Sato T, Matsui T, Sato M, Okada T, Yoshida H, Harada A, Mori K (2007). Transcriptional induction of mammalian ER quality control proteins is mediated by single or combined action of ATF6α and XBP1. Dev Cell 13, 365–376.

Yamamoto K, Suzuki N, Wada T, Okada T, Yoshida H, Kaufman RJ, Mori K (2008). Human HRD1 promoter carries a functional unfolded protein response element to which XBP1 but not ATF6 directly binds. J Biochem (Tokyo) 144, 477–486.

Ye J, Rawson RB, Komuro R, Chen X, Dave UP, Prywes R, Brown MS, Goldstein JL (2000). ER stress induces cleavage of membrane-bound ATF6 by the same proteases that process SREBPs. Mol Cell 6, 1355–1364.

Yoshida H, Haze K, Yanagi H, Yura T, Mori K (1998). Identification of the *cis*-acting endoplasmic reticulum stress response element responsible for transcriptional induction of mammalian glucose-regulated proteins; involvement of basic-leucine zipper transcription factors. J Biol Chem 273, 33741–33749.

Yoshida H, Matsui T, Hosokawa N, Kaufman RJ, Nagata K, Mori K. (2003). A time-dependent phase shift in the mammalian unfolded protein response. Dev Cell 4, 265–271.

Yoshida H, Matsui T, Yamamoto A, Okada T, Mori K (2001a). XBP1 mRNA is induced by ATF6 and spliced by IRE1 in response to ER stress to produce a highly active transcription factor. Cell 107, 881–891.

Yoshida H, Okada T, Haze K, Yanagi H, Yura T, Negishi M, Mori K (2001b). Endoplasmic reticulum stress-induced formation of transcription factor complex ERSF including NF-Y (CBF) and activating transcription factors 6a and 6b that activates the mammalian unfolded protein response. Mol Cell Biol 21, 1239–1248.

Yoshida H, Okada T, Haze K, Yanagi H, Yura T, Mori K (2000). ATF6 activated by proteolysis directly binds in the presence of NF-Y (CBF) to the *cis*-acting element responsible for the mammalian unfolded protein response. Mol Cell Biol 20, 6755–6767.

Yoshida H, Oku M, Suzuki M, Mori K (2006). pXBP1(U) encoded in XBP1 pre-mRNA negatively regulates unfolded protein response activator pXBP1(S) in mammalian ER stress response. J Cell Biol 172, 565–575.